AGU PUBLICATIONS

JGR

Journal of Geophysical Research: Oceans

RESEARCH ARTICLE

10.1002/2014JC010548

Development of HF radar inversion algorithm for spectrum estimation (HIAS)

Yukiharu Hisaki[1]

[1]Department of Physics and Earth Sciences, University of the Ryukyus, Okinawa, Japan

Key Points:
- A method to estimate ocean wave directional spectrum from HF radar is developed
- Estimate wave spectrum even at single radar Doppler spectrum cells
- This method is verified by comparing with in situ wave data

Correspondence to:
Y. Hisaki,
hisaki@sci.u-ryukyu.ac.jp

Citation:
Hisaki, Y. (2015), Development of HF radar inversion algorithm for spectrum estimation (HIAS), *J. Geophys. Res. Oceans*, *120*, doi:10.1002/2014JC010548.

Received 27 OCT 2014
Accepted 30 JAN 2015
Accepted article online 6 FEB 2015

Abstract A method for estimating ocean wave directional spectra using an HF (high-frequency) ocean radar was developed. This method represents the development of work conducted in previous studies. In the present method, ocean wave directional spectra are estimated on polar coordinates whose center is the radar position, while spectra are estimated on regular grids. This method can be applied to both single and multiple radar cases. The area for wave estimation is more flexible than that of the previous method. As the signal to noise (SN) ratios of Doppler spectra are critical for wave estimation, we develop a method to exclude low SN ratio Doppler spectra. The validity of the method is demonstrated by comparing results with in situ observed wave data that it would be impossible to estimate by the methods of other groups.

1. Introduction

An HF ocean radar observes surface currents and ocean waves by radiating HF radio waves to the sea surface. Surface currents are estimated by identifying the first-order Doppler peaks in the Doppler spectrum from HF ocean radar. The wave spectrum is estimated not only from the first-order, but also from the second-order scattering. Although estimating ocean wave spectra is important for both scientific and practical applications, few studies have sought to estimate ocean wave spectra from HF radar [e.g., *Lipa and Barrick*, 1986; *Wyatt*, 1990; *Howell and Walsh*, 1993; *Hisaki*, 1996; *Hashimoto et al*., 2003]. Here we developed a method for estimating ocean wave spectra from HF radar.

The relationship between the ocean wave spectrum and the second-order radar cross section is written in terms of the integral equation. The wave spectrum is inverted from the integral equation.

Methods have previously been developed for estimating ocean wave spectra. *Wyatt* [1990] and *Howell and Walsh* [1993] developed the inversion method, in which the integral equation is linearized by assuming the spectral form at higher frequencies. *Hisaki* [1996] and *Hashimoto et al*. [2003] developed a method of the inversion without linearization. An ocean wave directional spectrum at a given location can be estimated from two or more radars in these methods. The SN ratios in the Doppler spectra at the position in all radars must be high enough to estimate a wave spectrum. The area for wave estimation is thus limited in these methods.

A method to estimate ocean wave spectra using a single radar has also been developed [e.g., *de Valk et al*., 1999; *Hisaki*, 2005, 2006, 2009, 2014]. In this method, constraints such as the energy balance equation are used along with the relationship between the wave spectra and Doppler spectra. Wave spectra are estimated on radial grid points with the origin at the radar position in the method. *Hisaki* [2005] compared single radar-estimated wave data with in situ observed wave data; he then [*Hisaki*, 2006] described and verified the method from simulated Doppler spectra. The radar-wave data were significantly affected by the contamination of Doppler spectra, and so *Hisaki* [2009] developed a method of quality control for single radar-estimated wave data. He then [*Hisaki*, 2014] compared radar-estimated wave data with model-predicted wave data.

These methods are for a phase array system. Wave parameters are also estimated by the Coastal Ocean Dynamics Applications Radar (CODAR)-type HF radars, which is a compact antenna system. The CODAR-type HF radar systems, however, can only isolate the Doppler spectrum in range, not in azimuth. The wave parameters are estimated by applying the Pierson-Moskowitz model to second-order Doppler spectra in the CODAR radar system [*Long et al*., 2011].

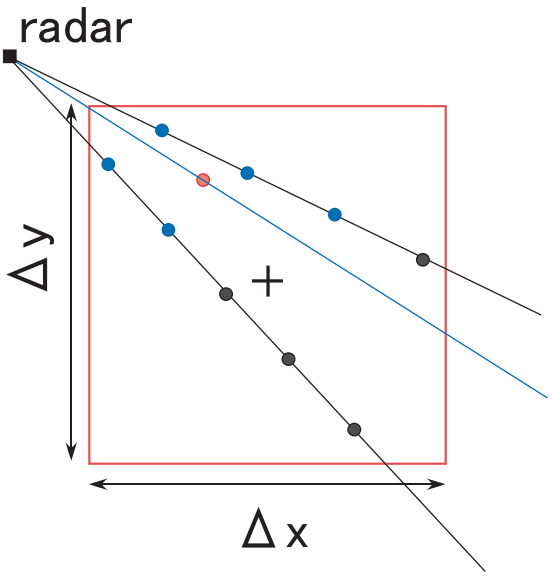

Figure 1. Schematic illustration of averaging Doppler spectra.

We extend the method in the present work, the wave spectra are estimated on the regular grid, and this method can be applied to both single and multiple radar array cases. The area for wave estimation is flexible, because wave spectra at positions where the Doppler spectra are not observed can be estimated in this method. The method is named HIAS (HF radar Inversion Algorithm for Spectrum estimation).

The objectives of this paper are as follows: (1) to describe the HIAS; (2) to describe the method for excluding low SN Doppler spectra; and (3) to validate the HIAS by comparing results with in situ observations.

This paper is organized as follows. The inversion method is described in section 2. In section 3, we present the observations by HF radar and the method to select Doppler spectra for wave estimation. The results of the selection of Doppler spectra and wave estimation are presented in section 4, and discussed in section 5. We summarize our conclusions in section 5.

2. Inversion Method

2.1. Constraints

The inversion method is almost the same as that described in *Hisaki* [2005, 2006]. The details are presented in *Hisaki* [2005, 2006, 2009]. The constraints for estimating wave spectra are as follows:

1. The relationship between the first-order Doppler spectrum and ocean wave directional spectrum.
2. The relationship between the second-order Doppler spectrum and ocean wave directional spectrum.
3. The energy balance equation under the assumption of stationarity.
4. Regularization constraints for spectral values in the wave frequency-wave direction plane.
5. The continuity equation of surface winds.
6. Regularization constraints for spectral values in the *x-y* plane.

2.2. Relationship Between the First and Second-Order Doppler Spectrum and Wave Spectrum

An observed Doppler spectral density $P(\omega_{DN})$ at a normalized Doppler frequency $\omega_{DN}=\omega_D/\omega_B$ is decomposed into

$$P_1(\omega_{DN})=P(\omega_{DN}) \qquad \omega_{dlN}(m) \le \omega_{DN} \le \omega_{duN}(m) \tag{1}$$

$$P_2(\omega_{DN})=P(\omega_{DN}) \qquad \omega_{DN} < \omega_{dlN}(m), \quad \omega_{DN} > \omega_{duN}(m) \tag{2}$$

where $P_1(\omega_{DN})$ and $P_2(\omega_{DN})$ are the first and second-order Doppler spectral densities, respectively. Parameters ω_D and ω_B are a radian Doppler frequency and the radian Bragg frequency, respectively. The normalized Doppler frequency ranges $\omega_{dlN}(m)$ and $\omega_{duN}(m)$ are lower and upper Doppler frequencies of the first-order scattering for the negative ($m=1$) and positive ($m=2$) Doppler frequency regions, respectively. They satisfy $\omega_{dlN}(m)<2m-3<\omega_{duN}(m)$, and are determined by identifying local minima around the two first-order scattering peaks [e.g., *Hisaki*, 2006, Figure 1]. The effect of the surface current on the Doppler spectrum is corrected. The Doppler spectra are shifted so that the first-order peaks are at the Bragg frequency.

The first and second-order Doppler spectral densities are written in terms of a normalized wave directional spectrum $G_N(\omega_N,\theta)=\omega_B(2k_0)^2G(\omega,\theta)$, in which k_0 is the radio wave number, ω is the radian wave

frequency, θ is the wave direction, and $\omega_N = \omega/\omega_B$ is the normalized frequency. The radian Bragg wave frequency is $\omega_B = (2gk_0)^{1/2}$ for deep water, where g is the gravitational acceleration. The subscript "N" denotes the normalized form by the Bragg parameters, such as ω_B and Bragg wave number $2k_0$.

The relationship between the first-order Doppler spectral density $P_1(\omega_{DN})$ and the normalized first-order radar cross section $\sigma_{1N}(\omega_{DN})$ is written in equations (2), (4), (5), and (6) in *Hisaki* [2006]; the relationship between the second-order Doppler spectral density $P_2(\omega_{DN})$ and the normalized second-order radar cross section $\sigma_{2N}(\omega_{DN})$ is written in equations (3), (4), (5), and (7) of that same study. The integrated first-order radar cross section is written as

$$\int_0^\infty \sigma_{1N}((2m-3)\omega_{DN})d\omega_{DN} = 2\pi G_N(1, \psi_B + (m-1)\pi), \qquad (m=1,2) \tag{3}$$

for deep water, where ψ_B is the radar beam direction. The second-order radar cross section is written in terms of $G_N(\omega_N, \theta)$, as

$$\sigma_{2N}(\omega_{DN}) = \int_{-\theta_L+\psi_B}^{\theta_L+\psi_B} K_I(\omega_{DN}, \theta_b) G_N(\omega_{1N}, \theta_1) G_N(\omega_{2N}, \theta_2) d\theta \tag{4}$$

where $\theta_b = \theta - \psi_B$ [*Hisaki*, 2006]. Meanwhile, the kernel function $K_I(\omega_{DN}, \theta_b)$ may be found in equation (29) in *Hisaki* [1996]. The integration range θ_L in equation (4) is π for $\omega_D^2 \leq 2$ for deep water, or equations (19), (20), and (21) in *Hisaki* [1996] for shallow water. The normalized wave frequencies and directions, (ω_{1N}, θ_1) and (ω_{2N}, θ_2), are those of wave components contributing to the second-order scattering. Details regarding the calculation of equation (4) are described in *Hisaki* [1996].

2.3. Energy Balance Equation

The energy balance equation under the assumption of the stationarity of wavefields is written as

$$\mathbf{C}_{gN} \cdot \nabla_N G_N(\omega_N, \theta) - S_{tN} = 0 \tag{5}$$

where $\mathbf{C}_{gN} = \partial\omega_N/\partial\mathbf{k}_N$ is the normalized group velocity vector of waves for wave frequency ω_N and wave number vector $\mathbf{k}_N$, ∇_N denotes the normalized horizontal gradient by $1/(2k_0)$, and S_{tN} denotes the total wave energy input [*Hisaki*, 2006]. The parameterization of the source function S_{tN} is the same as that in *Hisaki* [2006]. The propagation term in equation (5) is written in the regular coordinates $(x_N, y_N) = 2k_0(x, y)$ as

$$\mathbf{C}_{gN} \cdot \nabla_N G_N(\omega_N, \theta) = C_{gxN} \frac{\partial G_N(\omega_N, \theta)}{\partial x_N} + C_{gyN} \frac{\partial G_N(\omega_N, \theta)}{\partial y_N} \tag{6}$$

where C_{gxN} and C_{gyN} are the x and y components of the group velocity vector $\mathbf{C}_{gN}$. They are written as

$$(C_{gxN}, C_{gyN}) = C_{gN}(\cos\theta, \sin\theta) \tag{7}$$

where θ is the wave direction with respect to the x direction, and the counterclockwise is positive.

2.4. Other Constraints

The source function S_{tN} in equation (5) is not only dependent on the wave spectrum but also on the wind vector. The unknowns to be estimated are spectral values and wind vectors. The continuity equation of the nondivergent sea surface wind vector $\mathbf{u}_N = (u_{xN}, u_{yN}) = (u_N\cos\theta_w, u_N\sin\theta_w)$ is written as

$$\nabla_N \cdot \mathbf{u}_N = 0 \tag{8}$$

or

$$\frac{\partial(u_N\cos\theta_w)}{\partial x_N} + \frac{\partial(u_N\sin\theta_w)}{\partial y_N} = 0 \tag{9}$$

Equation (8) is the same as equation (15) in *Hisaki* [2006]. Equation (9) is written in the regular coordinate, while equation (16) in *Hisaki* [2006] is written in the polar coordinate.

The constraint written as

$$\mathbf{C}_{gN} \cdot \nabla_N G_N(\omega_N, \theta) = 0 \tag{10}$$

is used as a regularization constraint in the horizontal plane. This is in order to reduce the computation time [*Hisaki*, 2006].

2.5. Discretization

The wave spectral values $G_N(\omega_N, \theta) = G_N(\omega_N, \theta, x_N, y_N)$ are estimated on the $\omega_N - \theta - x_N - y_N$ space at

$$\log \omega_N = \log(\omega_N(k_f)) = \log(\omega_{minN}) + (k_f - 1)\log(\Delta_\omega), \qquad (k_f = 1, ..., M_f) \tag{11}$$

$$\theta = \theta(l_d) = -\pi + \frac{2\pi}{M_d}(l_d - 1), \qquad (l_d = 1, ..., M_d) \tag{12}$$

$$x_N = x_N(i_x) = \Delta x_N(i_x - 1) \qquad (i_x = 1, ..., N_x) \tag{13}$$

and

$$y_N = y_N(j_y) = \Delta y_N(j_y - 1) \qquad (j_y = 1, ..., N_y) \tag{14}$$

where k_f is the wave frequency index number, M_f is the number of frequencies, $\Delta_\omega > 1$ is the increment of the frequency, l_d is the wave direction index number, and M_d is the number of directions. The normalized spatial resolutions in the x and y directions are $\Delta x_N = 2k_0\Delta x$ and $\Delta y_N = 2k_0\Delta y$, respectively, where $(\Delta x, \Delta y)$ is the dimensional horizontal resolution. The number of grids in the x and y directions are N_x and N_y, respectively. Meanwhile, the index number of the grids in the x and y directions are i_x and j_y, respectively.

The discretized propagation term $\mathbf{C}_{gN} \cdot \nabla_N G_N(\omega_N, \theta)$ in equations (5) and (10) is $A_d(k_f, l_d, i_x, j_y)$, which is written as

$$\begin{aligned} A_d(k_f, l_d, i_x, j_y) &= \mathbf{C}_{gN} \cdot \nabla_N G_N(\omega_N, \theta) \\ &= C_{gxN}(k_f, l_d)\frac{G_N(k_f, l_d, i_x + m_{x1}, j_y) - G_N(k_f, l_d, i_x - m_{x2}, j_y)}{(m_{x1} + m_{x2})\Delta x_N} \\ &+ C_{gyN}(k_f, l_d)\frac{G_N(k_f, l_d, i_x, j_y + m_{y1}) - G_N(k_f, l_d, i_x, j_y - m_{y2})}{(m_{y1} + m_{y2})\Delta y_N} \end{aligned} \tag{15}$$

The continuity equation (equation (8)) is discretized as

$$\frac{u_{xN}(i_x + m_{x1}, j_y) - u_{xN}(i_x - m_{x2}, j_y)}{(m_{x1} + m_{x2})\Delta x_N} + \frac{u_{yN}(i_x, j_y + m_{y1}) - u_{yN}(i_x, j_y - m_{y2})}{(m_{y1} + m_{y2})\Delta y_N} = 0 \tag{16}$$

where m_{x1}, m_{x2}, m_{y1}, and m_{y2} in equations (15) and (16) are 0 or 1. The value $m_{x1} = 0$ for $i_x = N_x$, $m_{x2} = 0$ for $i_x = 1$, $m_{y1} = 0$ for $j_y = N_y$, and $m_{y2} = 0$ for $j_y = 1$. Otherwise, they are 1.

The regularization constraint is expressed as

$$\begin{aligned} &\log(G_N(k_f + 1, l_d)) + \log(G_N(k_f - 1, l_d)) \\ &+ \log(G_N(k_f, l_d - 1)) + \log(G_N(k_f, l_d + 1)) \\ &- 4\log(G_N(k_f, l_d)) = 0 \qquad \text{for} \quad 1 < k_f < M_f \qquad \text{and} \quad 1 \le l_d \le M_d \\ &\text{or} \quad \log(G_N(k_f, l_d - 1)) + \log(G_N(k_f, l_d + 1)) \\ &- 2\log(G_N(k_f, l_d)) = 0 \qquad \text{for} \quad k_f = 1, M_f \end{aligned} \tag{17}$$

where $G_N(k_f, 0) = G_N(k_f, M_d)$ and $G_N(k_f, M_d + 1) = G_N(k_f, 1)$.

2.6. Summary of Constraints

Constraints 1 in section 2.1 are equations (2), (4), (5), and (6) in *Hisaki* [2006] and equation (3); constraints 2 in section 2.1 are equations (3–5) and (7) in *Hisaki* [2006] and equation (4). The discretization of equation (4) is described in *Hisaki* [1996]. Constraint 3 in section 2.1 is equation (5). The source function, including the nonlinear source function, is discretized as section 3b in *Hisaki* [2006], and the propagation term is discretized as equation (15). Constraint 4 is discretized as equation (17), and constraint 5 in section 2.1 is equation (8). The discretization of equation (8) is equation (16). Constraint 6 in section 2.1 is equation (10), and the

discretization of equation (10) is equation (15). The difference here from *Hisaki* [2005, 2006, 2009, 2014] is the expression of the horizontal gradient ∇_N.

2.7. Doppler Spectrum Averaging

If Doppler spectra are estimated on regular grid points, the beam direction ψ_B in equations (3) and (4) is the direction of the grid from the radar. However, Doppler spectra are sampled on polar grids. The origin of the polar grids is the radar position, the radial resolution is the range resolution, and the azimuthal resolution is the beam step of the HF radar.

Figure 1 shows a schematic illustration of Doppler spectra averaging. The black rectangle symbol shows the position of the radar, and the beam directions are indicated by the black lines. Only two beam directions are indicated for simplicity. The red-line rectangle shows the cell, and the symbol + at the center of the rectangle is the regular grid point. Blue and black circles on the beam direction lines in Figure 1 represent sampling points of the Doppler spectra.

We assume that ocean waves are statistically homogeneous in the rectangle cell. The Doppler spectra sampled on the blue circles are used for wave estimation; those sampled on the black circles are not used for wave estimation, however, because of low SN ratios. The Doppler spectra sampled on the blue circles are averaged. The cell-averaged Doppler spectra $P(\omega_{DN})$ in equations (1) and (2) are used for the inversion. The mean position of Doppler spectra for wave estimation is calculated and shown as the red circle in Figure 1. The direction of the mean position from the radar is the beam direction $\psi_B = \psi_B(i_x, j_y, m_r)$ ($m_r = 1,\ldots,M_r$) in equations (3) and (4), indicated by the blue line in Figure 1. M_r is the number of radars used, and m_r is the radar index number.

2.8. Optimization Problem

The number of unknowns $N_u = N_s + 2N_g$, where $N_g = N_x N_y$ is the number of regular grid points, and $N_s = M_f M_d N_g$ is the number of total spectral values of the wave spectrum. The value of $2N_g$ is the number of wind speeds and directions to be estimated. The total number of the constraints N_t in section 2.1 is

$$N_t = 3N_s + N_g + K_{DF} + K_{DT} \tag{18}$$

$$K_{DT} = \sum_{m_r=1}^{M_r} \sum_{i_x=1}^{N_x} \sum_{j_y=1}^{N_y} K_D(i_x, j_y, m_r) \tag{19}$$

where $K_D(i_x, j_y, m_r)$ is the number of cell-averaged Doppler spectral values for wave estimation at the position (i_x, j_y) and the radar index number m_r (these are explained in section 2.7). K_{DF} is the number of the first-order scattering for the inversion, and it is $1 \le K_{DF} \le N_g M_r$. The number of constraints of 1, 2, 3, 4, 5, and 6 are K_{DF}, K_{DT}, N_s, N_s, N_g, and N_s, respectively.

The number of constraints is larger than the number of unknowns (i.e., $N_t > N_u$). The unknowns, **s**, are estimated by seeking the values to minimize the objective function, as

$$U(\mathbf{s}) = \frac{1}{2} \sum_{K=1}^{N_t} [\lambda_w(M, K) F_k(\mathbf{s})]^2 \tag{20}$$

The N_u-dimensional vector **s** denotes the logarithm of ocean wave spectral values ($\log(G_N)$), wind speeds ($\log(u_N)$), and wind directions (θ_w). The function F_K denotes the constraints in section 2.1. The parameter $\lambda_w(M, K)$ is the weight, which should be given adequately. The index M denotes the type of constraint, while the number K is the index number of the equations. Here index number M ($M = 1,\ldots,6$) is the same as the constraint number in section 2.1. For example, $M = 3$ is constraint 3 in section 2.1 (energy balance equation). In this case, the range of K for M is

$$K_{rg}(M-1) < K \le K_{rg}(M) \tag{21}$$

$$K_{rg}(M) = K_{rg}(M-1) + N_c(M) \tag{22}$$

where $K_{rg}(0) = 0$, and $N_c(M)$ is the number of constraints for M. The values of $N_c(M)$ are $N_c(1) = K_{DF}$, $N_c(2) = K_{DT}$, $N_c(3) = N_c(4) = N_c(6) = N_s$, and $N_c(5) = N_g$. The weight $\lambda_w(M, K)$ is dependent on M only for $M \ge 3$.

The contribution to the solution of the cell-averaged Doppler spectrum from many Doppler spectra is large, while the contribution of averaged Doppler spectrum from a few Doppler spectra is small. The weight $\lambda_w(M,K)$ for $M = 1$ and 2 is dependent on the number of Doppler spectra for averaging, explained in section 2.7. The weight is written as

$$\lambda_w(M,K) = \lambda_{wM} N_d(i_x, j_y, m_r) \qquad (M = 1, 2) \tag{23}$$

where $N_d(i_x j_y m_r)$ is the number of Doppler spectra for averaging in the cell (i_x, j_y) and the radar index number m_r. The parameters λ_{wM} ($M = 1, 2$) are adequately given. The number of Doppler spectra for constraints 1 and 2 in section 2.1 are the same here. The algorithm to solve the optimization problem of equation (20) is the same as in *Hisaki* [2006, 2009].

3. Data Analysis

3.1. Observation

The Doppler spectra from 17 April 1998to 13 May 1998, observed to the east of Okinawa Island, Japan, were used for analysis. Observations are described in *Hisaki et al*. [2001] and *Hisaki* [2002]. Radio frequency was 24.5 MHz, and Bragg frequency $f_B = \omega_B/(2\pi)$ was 0.506 Hz. The sampling interval of radar signals was 0.5 s, which gave a Nyquist frequency of 1 Hz. Resolution in the Doppler frequency was 1/128 Hz.

Figure 2 shows the HF radar observation area. In the figure, the radar locations are A (26.12° N, 127.76° E) and B (26.31°N, 127.84°E). Beam directions of radar A are from 43.5°T to 126°T. Those of radar B are from 118.5°T to 201°T. Beam step is 7.5°, number of beam directions for each radar is 12, and range resolution is 1.5 km. The black triangles and squares in Figure 2 are sampling points of Doppler spectra from radars A and B, respectively. The temporal resolution of observed Doppler spectra was 2 h. The period of analysis was from 0 LST (Local Standard Time) 17 April 1998to 22 LST 13 May 1998.

Waves were measured at position N in Figure 2 using the Ultrasonic Wave Gauge (USW) (Port and Harbour Research Institute, Japan). The USW measures surface waves at 0.5 s intervals. Significant wave heights were estimated using the zero-up-cross method based on 20 min of observation of surface displacements at 2 h intervals [e.g., *Hisaki*, 2007]. The water depth at N in Figure 2 was 46 m.

The regular grids for wave estimation are indicated in Figure 2. The x direction is eastward and the y direction northward. Number of grid points is $N_x = N_y = 4$ for both x and y directions; grid size is $\Delta x = \Delta y = 9$ km. Symbols + in Figure 2 designate the centers of the regular cells processed from radial grids. The grid center position for $i_x = j_y = 1$ is (25.95°N, 127.9°E).

The wave parameters estimated by the HF radar were the same as those in *Hisaki* [2009]. The wave frequency parameters in equation (11) were $\Delta_\omega = 1.15$, $\omega_{min}/(2\pi) = 0.049$ Hz, and $M_f = 21$. The maximum wave frequency was $\omega_{max}/(2\pi) = 0.813$ Hz; the wave direction parameter in equation (12) was $M_d = 18$; and the number of unknowns was $N_u = 6080$.

The Doppler frequency ranges of the second-order scattering for wave estimation were $0.61 \le |\omega_{DN}| \le 0.94$ and $1.06 \le |\omega_{DN}| \le 1.39$ at the 0.03 interval, and $K_D(i_x, j_y, m_r) = 48$ for $N_d(i_x, j_y, m_r) > 0$. The normalized Doppler frequency interval 0.03 is different from that of measured Doppler spectra $(1/(128 f_B))$. The value $P_2(\omega_{DN})$ for the cell-averaged Doppler spectrum was interpolated with respect to the Doppler frequency.

The noise floor was subtracted from the cell-averaged Doppler spectrum, and evaluated by averaging the lowest quarter of the Doppler spectral values. The evaluated noise floor was much smaller than the second-order Doppler peak values. The mean ratio of the second-order Doppler peak to the noise floor was 13 dB.

The weight in equations (20) and (23) was $\lambda_{w1}/\lambda_{w2} = (\nu_1/\nu_2)^{1/2}$, where ν_1 is the degree of freedom of the integrated first-order Doppler spectrum, and ν_2 is the degree of freedom of the second-order Doppler spectrum. Sampling variability in the spectral estimate is inversely proportional to the square of the degree of freedom. Here the values were $\nu_1 = 72$ and $\nu_2 = 11$ [e.g., *Hisaki*, 2005, 2009]. Other weights were $\lambda_{w2} = 10$, and $\lambda_w(M,K) = 1$ for $M \ge 3$. We calculated for different values of the weights, and wave estimation results were similar to those presented in this paper.

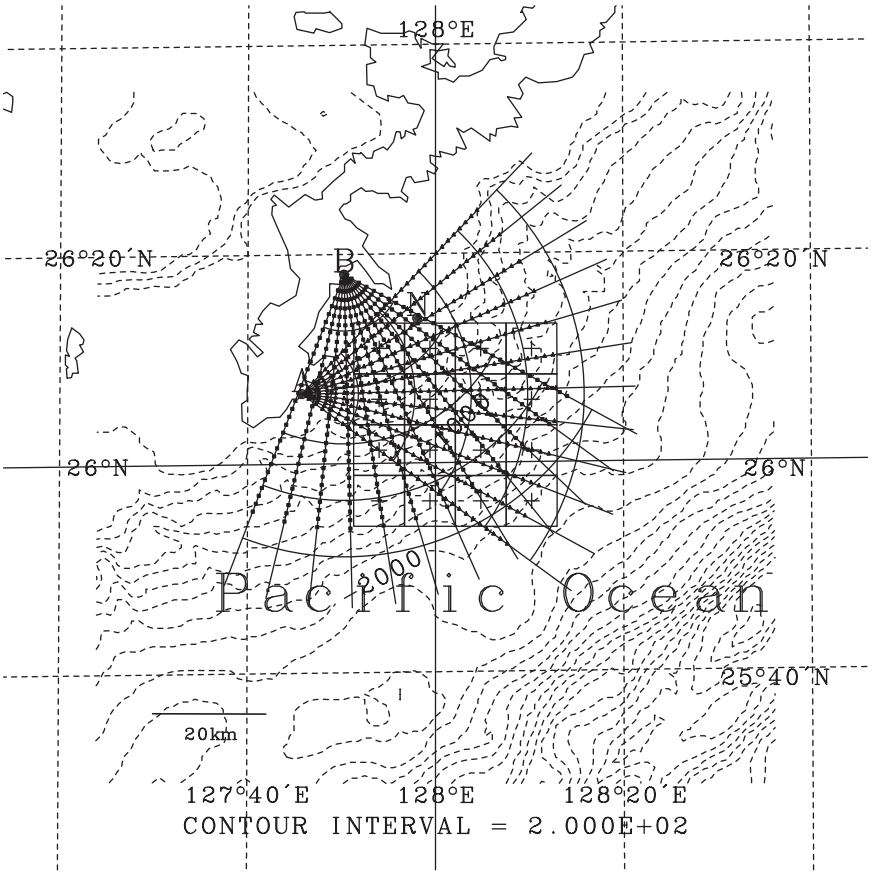

Figure 2. Map of HF radar observation area.

3.2. Selection of Doppler Spectra

If a Doppler spectrum is significantly contaminated by noise, radar-estimate wave data will not be good. The selection of Doppler spectra is critical for wave estimation. The methods and criteria for selecting Doppler spectra are as follows:

1. Manual selection.

2. Identification of first-order scattering.

3. Classification of Doppler spectra by the self-organizing map (SOM) analysis.

4. Ratio of the second-order scattering to the first-order scattering.

A manual selection of Doppler spectra may be useful. However, it is impossible to select manually from too many Doppler spectra. This method was applied only for Doppler spectra averaged over the observation period. Figure 3 shows examples of averaged Doppler spectra from radar A and beam direction 96°T. The corresponding distances of Doppler spectra from radar A are from 3 to 51 km in Figure 3.

The second-order scattering is not so clear in averaged Doppler spectra from 3 km (red line) to 9 km (red line) in Figure 3. The Doppler peaks at $\omega_{DN} \simeq -0.4$ for longer distance are spurious, because this Doppler peak becomes larger as distance increases. The Doppler peaks at $\omega_{DN} \simeq -1.7$ for longer distances are also spurious. The distance of the Doppler spectra passed criteria 1 for this radar A and beam direction 96° T was from 10.5 to 30 km. This selection was performed for both radars (A and B), and for 12 beam directions for each radar manually. The ranges of the distance of Doppler spectra from the radar were decided for each radar and beam direction manually from Doppler spectra averaged over the observation period. Out-of-range Doppler spectra were not used for wave estimation. Some other spectra within the range were also not used for wave estimation.

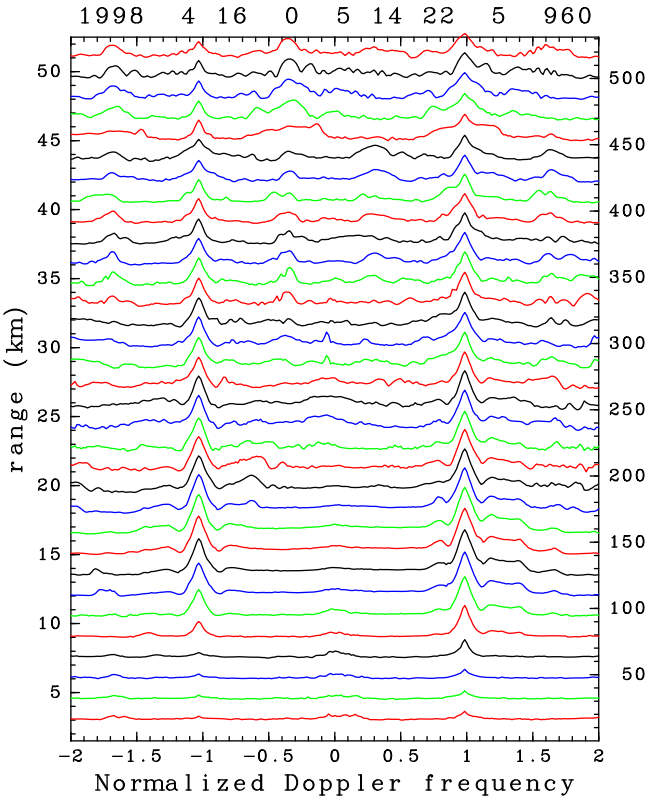

Figure 3. Averaged Doppler spectra for various ranges (distances from the radar). The radar is A in Figure 2, and the beam direction is 96°T. The left vertical axis indicates the distance of each Doppler spectrum from the radar. The right vertical axis indicates the relative signal intensity in decibels.

At the least, the first-order scattering peaks must be identified for wave estimation. In addition, the first-order scattering Doppler frequency ranges $\omega_{dlN}(m) < 2m-3 < \omega_{duN}(m)$, $(m = 1, 2)$ must be identified. They are identified by seeking the local minima of the running average Doppler spectrum. Doppler spectra are running averaged with respect to Doppler frequencies. If the Doppler frequencies of local minima are sensitive to the running average number, we consider that the first-order scattering Doppler frequency ranges $(\omega_{dlN}(m), \omega_{duN}(m))$ are not identified.

The SOM method described in *Liu and Weisberg* [2005] and *Hisaki* [2013] was used to classify the Doppler spectra. The purpose of classifying the Doppler spectra is to isolate those spectra contaminated by noise.

SOM analysis evaluates the weight vectors and the best-matching unit (BMU). The BMU is the group number, and the weight vector shows the pattern of the group. The SOM array is the array of weight vectors. The distance between two units in the SOM array indicates the similarity of the groups. For example, in the case of the $K_S \times K_S$ SOM array, the BMU is from 1 to K_S^2. The distance between BMU = 1 and BMU = 2 is 1, and the distance between BMU = 1 and BMU = $K_S + 1$ is also 1, this shows that the groups of BMU = 2 and BMU = $K_S + 1$ are the most similar to the group of BMU = 1. The distance between BMU = 1 and BMU = K_S^2 is $(K_S-1)\sqrt{2}$, which shows that the groups of BMU = 1 and BMU = K_S^2 are the most dissimilar to each other.

A Doppler spectrum is converted to

$$Q(\omega_{DN}) = 10\log_{10}\left(\frac{P((2m-3)\omega_{DN})}{P(2m-3)}\right) \qquad (m=1 \quad \text{or} \quad 2) \tag{24}$$

where $m = 1$ for $P(-1) > P(1)$, and $m = 2$ for $P(-1) \le P(1)$. The maximum value of $Q(\omega_{DN})$ is 0 dB at $\omega_{DN} = 1$. This conversion aims to avoid to classify the Doppler spectra of $P(-1) > P(1)$ and those of $P(-1) < P(1)$ into different groups. The Doppler spectrum is normalized by the peak value of the Doppler spectrum, and then converted into decibels. The Doppler frequency range for the classification is $\omega_{pdN} \le |\omega_{DN}| \le \omega_{qdN}$, where ω_{pdN} and ω_{qdN} are given parameters.

The first 1000 Doppler spectra that satisfied criteria 1 and 2 were used for classification. They were classified into $K_S \times K_S$ groups. We selected the groups that included the Doppler spectra contaminated by noise. The 1000 Doppler spectra were used to establish group numbers (BMU) and typical patterns (weight vectors) of Doppler spectra for each group. Other Doppler spectra that satisfied criteria 1 and 2 were classified into any group of $K_S \times K_S$ groups. If the Doppler spectrum belonged to the noisy Doppler spectrum groups, it was not used for wave estimation.

The parameter

$$R_{12} = \left[8 \frac{\int_{-\infty}^{\infty} P_2(\omega_{DN}) / w(\omega_{DN}) d\omega_{DN}}{\int_{-\infty}^{\infty} P_1(\omega_{DN}) d\omega_{DN}} \right]^{1/2} \simeq \left[\frac{8 \sum_{m=1}^{2} \int_{\omega_{pdN}}^{\omega_{qdN}} P_2((2m-3)\omega_{DN}) / w(\omega_{DN}) d\omega_{DN}}{\sum_{m=1}^{2} \int_{\omega_{dlN}(m)}^{\omega_{duN}(m)} P_1(\omega_{DN}) d\omega_{DN}} \right]^{1/2} \quad (25)$$

where $w(\omega_{DN})$ is the weighting function for normalized Doppler frequency ω_{DN} defined in *Barrick* [1977] was evaluated for the Doppler spectra that passed criteria 1–3. The value of R_{12} can be seen as a rough approximation of the wave height [*Barrick*, 1977]. If the value of R_{12} for a Doppler spectrum was much larger than those of other Doppler spectra, that spectrum was excluded from wave estimation.

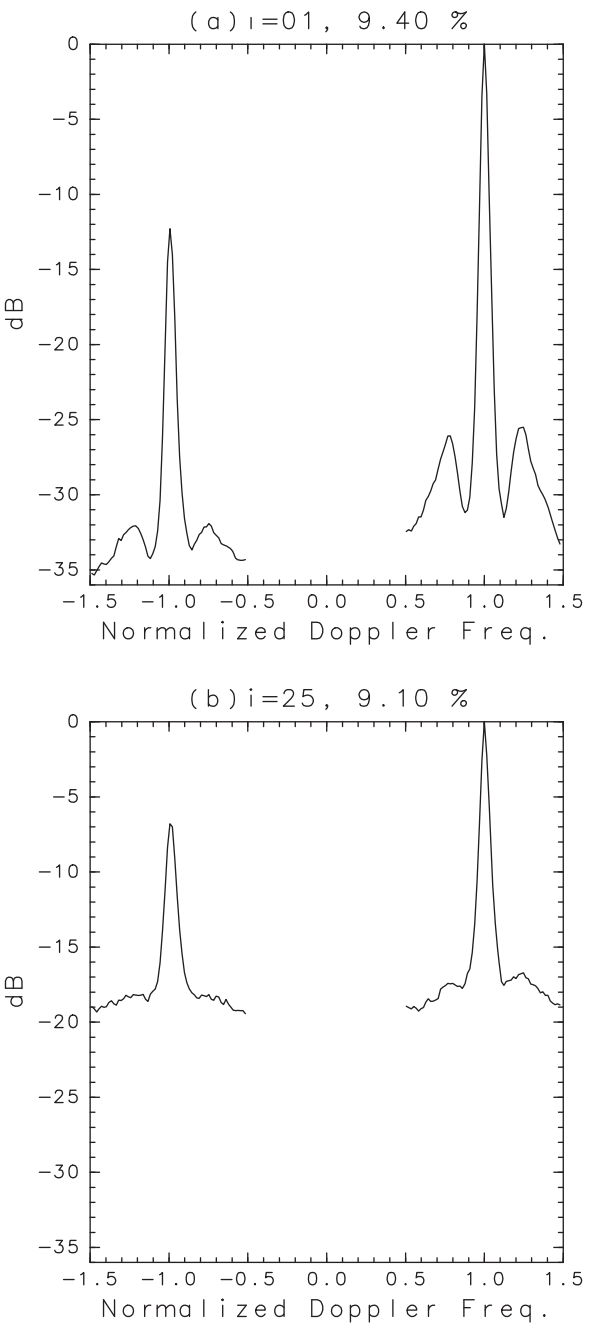

Figure 4. Weight vectors, which are explained in section 3.2, for (a) BMU = 1 and (b) BMU = 25, classified $Q(\omega_{DN})$ in equation (24) by the SOM.

4. Results

4.1. Doppler Spectrum

The SOM was applied for $Q(\omega_{DN})$ in equation (24). The parameters were $M_S = 5$, $\omega_{pdN} = 0.5$, and $\omega_{qdN} = 1.5$.

Figure 4 shows the weight vectors of SOM classification of $Q(\omega_{DN})$ in equation (24) for BMU = 1 and BMU = 25. The weight vector shows the classification pattern for each BMU. The examples in Figure 4 are frequent patterns. The distance between the BMU = 1 and BMU = 25 was the longest in the SOM array, which means that these patterns were opposite to each other. The frequency for BMU = 1 was 9.4% (Figure 4a), which means that 1000 × 0.094 = 94 Doppler spectra belonged to this group. The frequency for BMU = 25 was 9.1%. The second-order scattering peaks are clear in Figure 4a, and not in Figure 4b. The noise floor was about −35 dB in Figure 4a, and about −19 dB in Figure 4b. Thus, the group BMU = 25, and groups close to it, such as BMU = 19, 20, and 24, were the noisy Doppler spectra groups.

Figure 5 shows examples of Doppler spectra $P(\omega_{DN})$ for BMU = 1 and 25. The second-order Doppler peaks can be seen in most of the Doppler spectra for BMU = 1 (Figure 5a). They are quasiabsent for BMU = 25 (Figure 5b). The SOM is useful for isolating the noisy Doppler spectra. However, it is better to use the SOM in combination with other methods, such as a method of criteria 4, to select Doppler spectra for wave estimation.

The number of Doppler spectra for wave estimation per observation is

$$N_{DT}=\sum_{m_r=1}^{M_r}\sum_{i_x=1}^{N_x}\sum_{j_y=1}^{N_y}N_d(i_x,j_y,m_r)=\sum_{m_r=1}^{M_r}N_{DR}(m_r)=\sum_{i_x=1}^{N_x}\sum_{j_y=1}^{N_y}N_{cd}(i_x,j_y) \quad (26)$$

where $N_d(i_x,j_y,m_r)$ is used in equation (23), $N_{DR}(m_r)$ is the number of Doppler spectra available for wave estimation of the radar m_r, and $N_{cd}(i_x,j_y)$ is the number of Doppler spectra in the cell (i_x, j_y) available for wave estimation.

Figure 6a shows the time-averaged values of $N_{cd}(i_x,j_y)$. The mean values of $N_{cd}(i_x,j_y)$ were 0 at $(i_x, j_y) = (1, 1)$, (3, 1), (4, 1), and (4, 2): there were no Doppler spectra for wave estimation over the entire observation period at these cells. The mean values of $N_{cd}(i_x,j_y)$ were less than 1 at $(i_x, j_y) = (1, 4)$, (4, 3), and (4, 4), which means that there were no Doppler spectra during most of the observation period at these cells. The mean values of $N_{cd}(i_x,j_y)$ were larger at $(i_x, j_y) = (1, 3)$ and (2, 3), which showed that SN ratios of Doppler spectra in the cells were higher than in other cells.

Figure 6b and c show the time mean values of the numbers of Doppler spectra available for wave estimation for radar A ($N_d(i_x,j_y,1)$) and radar B ($N_d(i_x,j_y,2)$), respectively. The mean value of $N_d(i_x,j_y,1)$ was 0 at cells $(i_x, j_y) = (1, 1)$, (3, 1), (4, 1), (4, 2), (4, 3), (1, 4), (2, 4), (3, 4), and (4, 4). The value of $N_d(i_x,j_y,2)$ was 0 at cells $(i_x, j_y) = (1, 1)$, (2, 1), (3, 1), (4, 1), (3, 2), and (4, 2). Cells $(i_x, j_y) = (2, 1)$, (4, 3), (1, 4), (2, 4), (3, 4), and (4, 4) were single radar Doppler spectrum cells during the observation period. The regular cell $(i_x, j_y) = (2,4)$ was closest to the in situ wave observation point.

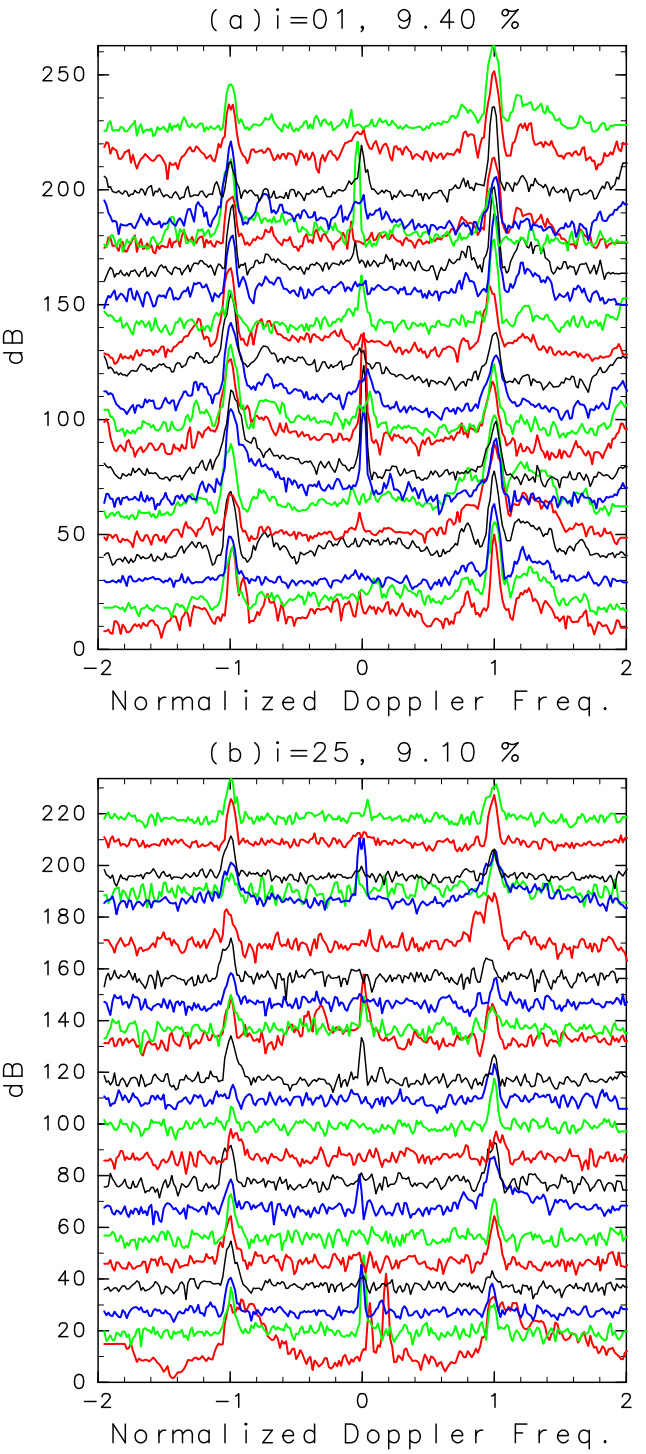

Figure 5. Examples of Doppler spectra $P(\omega_{DN})$ for (a) BMU = 1 and (b) BMU = 25, classified $Q(\omega_{DN})$ in equation (24) by the SOM. The vertical axis indicates the relative signal intensity in decibels.

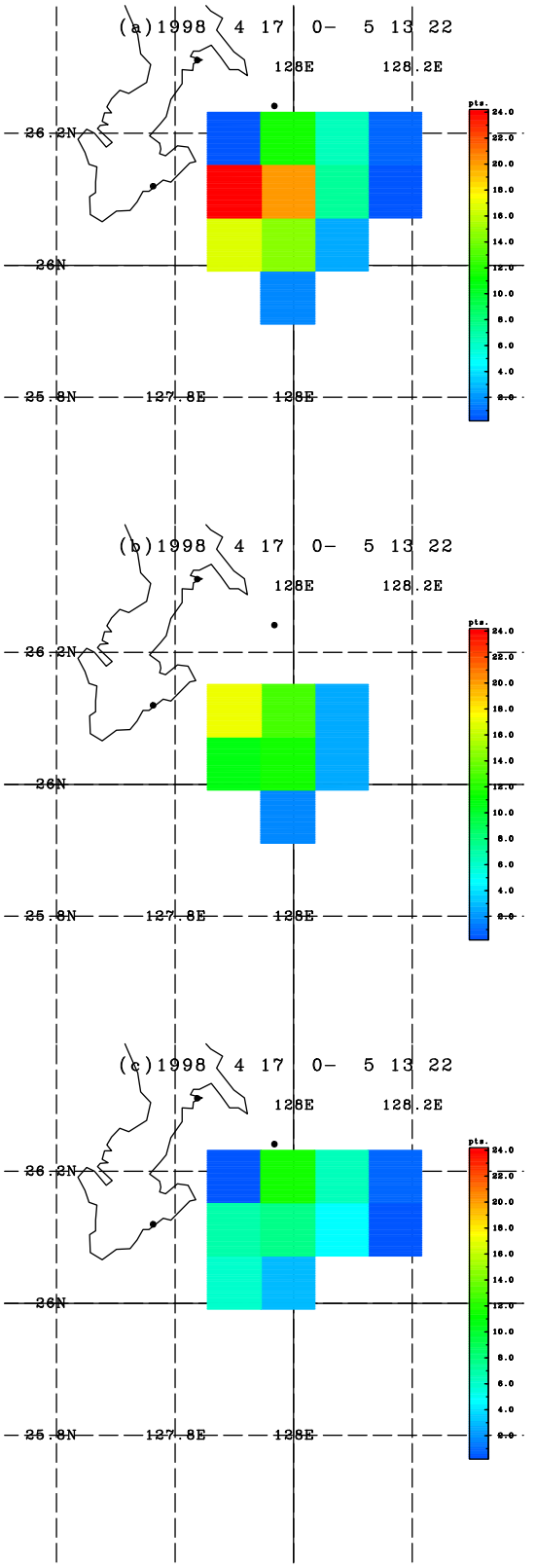

Figure 6. (a) Time-averaged value of the number of available Doppler spectra for wave estimation per observation, $N_{cd}(i_x, j_y)$ in equation (26); (b) same as Figure 6a but for radar A ($N_d(i_x, j_y, 1)$); (c) same as Figure 6a but for radar B ($N_d(i_x, j_y, 2)$).

Figure 7a shows the time series of the number of total Doppler spectra for both radars (N_{DT}), radar A ($N_{DR}(1)$) and radar B ($N_{DR}(2)$), in equation (26) for wave estimation. Figure 7b shows the time series of the number of Doppler spectra $N_{cd}(i_x, j_y)$ for wave estimation in the regular cell at $(i_x, j_y) = (2,4)$. There were no Doppler spectra for wave estimation from 18 LST to 22 LST 20 April 1998 (Figure 7a). Ocean wave spectra were therefore not estimated at that time. The time-averaged value of N_{DT} was 106 for $N_{DT} > 0$, which means that 106 Doppler spectra, on average, were used for wave estimation. The time-averaged value of $N_{cd}(2,4)$ was 12, which means that, on average, 12 Doppler spectra in the regular cell $(i_x, j_y) = (2,4)$ were used for wave estimation. The value of N_{DT} varied with time. The maximum was 144, and the minimum was 40 for $N_{DT} > 0$. The maximum of $N_{cd}(2,4)$ was 18 and the minimum was 0 for $N_{DT} > 0$. The beam direction $\psi_B(i_x, j_y, m_r)$ also varied with time.

4.2. Wave Estimation

Figure 8 shows examples of ocean wave directional spectra $2\pi G(2\pi f, \theta)(f = \omega/(2\pi))$ in cell $(i_x, j_y) = (2,4)$, which was closest to the in situ wave observation point. Although the Doppler spectra of radar B only were included in the cell, the wave directional spectrum could be estimated. The estimated wave height is 1.76 m in Figure 8a, while the in situ measured wave height was 1.42 m, relatively high for the observation period. The estimated wave height is 0.96 m in Figure 8b, while the in situ measured wave height was 0.97 m.

The peak wave direction is about $\theta = 120^\circ$ in Figure 8a, which means that the dominant wave propagated northwestward. The peak wave direction is about $\theta = -160^\circ$ in Figure 8b, which means that the dominant wave propagated west-south westward. The waves are propagated from offshore.

The hindcast dominant wave direction at $(26^\circ\text{N}, 128^\circ\text{E})$ by JMA (Japan Meteological Agency) was east-southeast at 9 LST (0 UTC) 21 April, and the wind at the location was southeasterly. The hindcast dominant wave directions were east at 9 LST 7 and 8 May, and winds were southerly [*Japan Meteological Agency*, 1999]. Dominant wave directions of radar-estimated wave spectra agreed with those predicted by JMA.

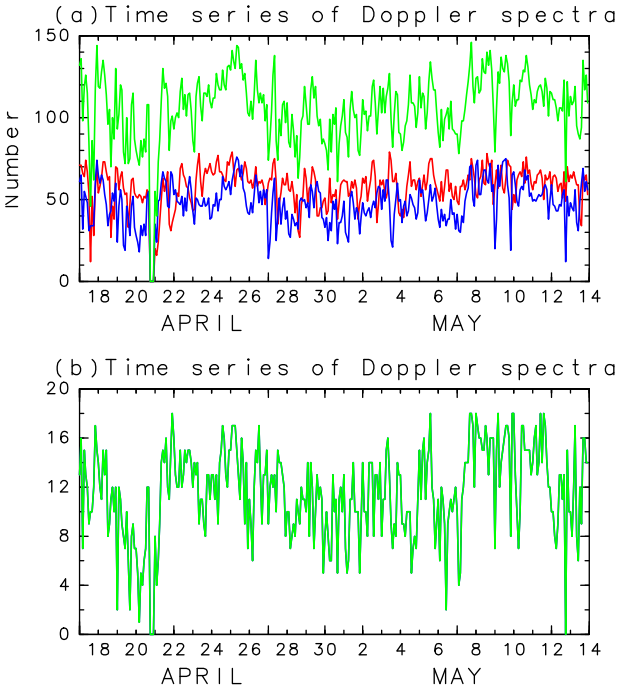

Figure 7. (a) Time series of the number of Doppler spectra for wave estimation. Green: N_{DT} in equation (26). Red: Radar A ($N_{DR}(1)$). Blue: Radar B ($N_{DR}(2)$). (b) Time series of the number of Doppler spectra for wave estimation in the cell closest to the wave observation point. $N_{cd}(i_x, j_y)$ at $(i_x, j_y) = (2, 4)$.

Figure 9 shows the comparison between USW wave heights (H_s) and radar-estimated wave heights (H_r) in the cell closest to the in situ observation point. The maximum in situ wave height H_s was 1.57 m at 8 LST 21 April. The wave conditions were calm during the observation period. There were 321 comparisons. The correlation coefficient between H_s and H_r was 0.82 with an rms difference of 0.22 m. There was good agreement between USW wave heights and radar-estimated wave heights. The linear regression line in Figure 9b is $H_r = 1.14\ H_s + 0.045$, indicating that radar-estimated wave heights were slightly higher than USW wave heights.

Figure 10 shows the mean radar-estimated wave heights during the observation period. Mean wave heights ranged from 1 to 1.2 m. Mean wave height was higher further offshore.

5. Discussion and Conclusions

We developed a method for estimating ocean wave spectra from HF radar, called the HIAS (HF radar Inversion Algorithm for Spectrum estimation). Doppler spectra used for estimating ocean wave spectra must not be contaminated by noise. However, many Doppler spectra are noise contaminated. We used the SOM, along with the other criteria listed in section 3.2 to select Doppler spectra.

We assumed that the wavefield was statistically homogeneous in the regular grid cell of $\Delta x \times \Delta y$. The Doppler spectra available for wave estimation change over time. The Doppler spectrum data are tractable due to the assumption, however, because we only averaged Doppler spectra for wave estimation and positions. If homogeneity in the cell is not assumed, the cell-averaged Doppler spectrum would be expressed in terms of the wave spectra at the four grid points surrounding the cell. The inversion then becomes more complicated than that used in the present method.

Six kinds of constrains were used in the present method. It may be possible to estimate wave spectra without the energy balance equation (constraint 3). We also estimated wave spectra for the same weights $\lambda_w(M,K)$ as in section 3.1, except for $\lambda_w(3,K) = 0$, which means that the energy balance equation was not incorporated into the inversion. The correlation coefficient between in situ measured wave heights (H_s) and the radar-estimated wave heights (H_r) was 0.71 with an rms difference of 0.35 m. This result was poorer than that in section 4.2. Therefore, we conclude that it is necessary to incorporate the energy balance equation into the inversion.

The regular cells were classified into three groups. The first was the dual radar Doppler spectrum cell, in which $N_d(i_x, j_y, 1) \neq 0$ and $N_d(i_x, j_y, 2) \neq 0$. The second the no-radar Doppler spectrum cell, in which $N_d(i_x, j_y, 1) = N_d(i_x, j_y, 2) = 0$. Finally, the third was the single radar Doppler spectrum cell, which is only $N_d(i_x, j_y, 1) = 0$, or $N_d(i_x, j_y, 2) = 0$. These cell types vary with time. The regular cell at $(i_x, j_y) = (2,4)$ was a single radar Doppler spectrum cell for most of the observation period; this cell $(i_x, j_y) = (2,4)$ was never a dual radar Doppler spectrum cell.

The agreement between in situ measured wave heights and radar-estimated wave heights was good at this cell. Previous methods for estimating wave spectra from HF radar developed by other groups [*Wyatt*, 1990;

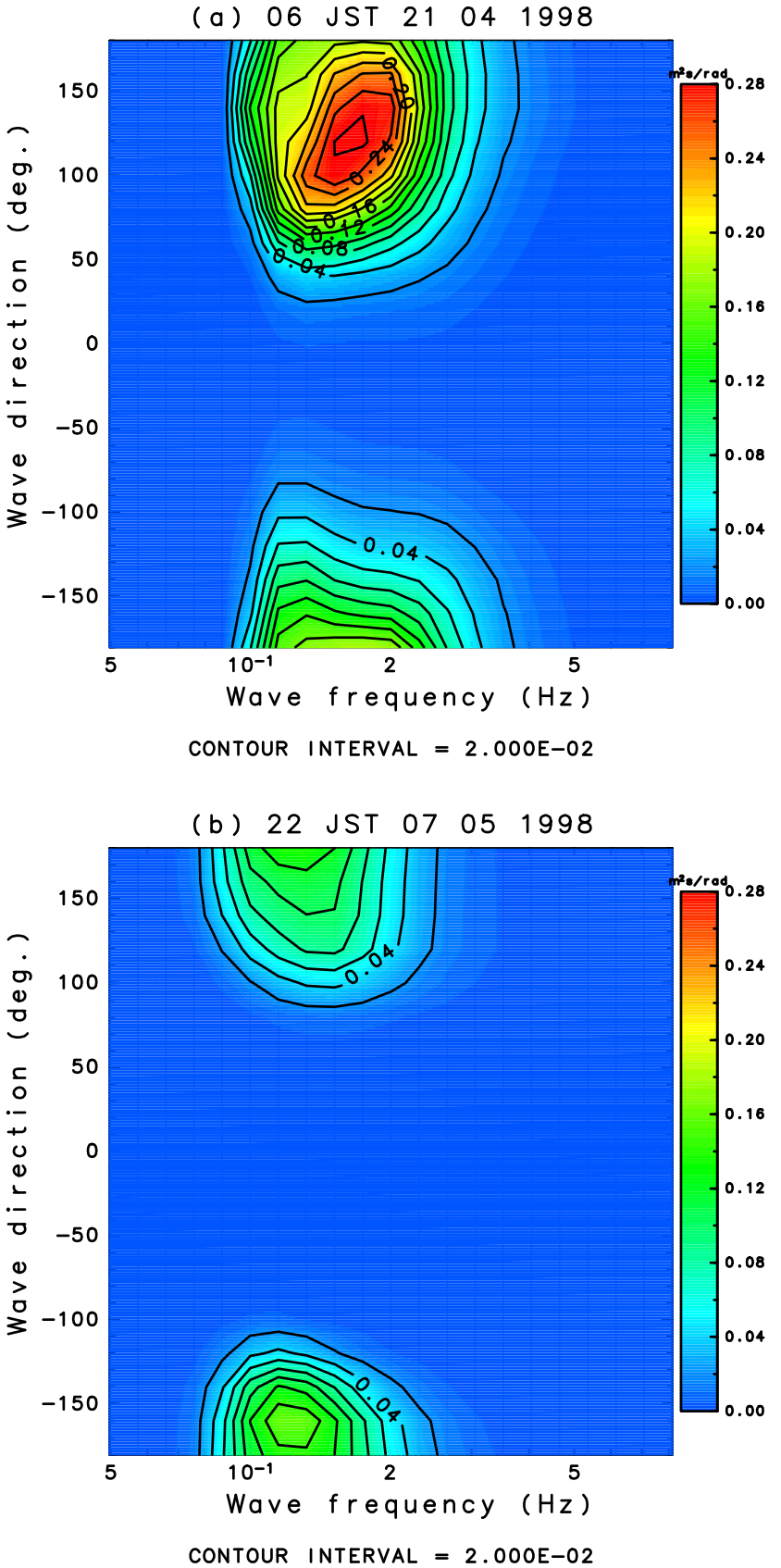

Figure 8. Examples of ocean wave spectra $2\pi G(2\pi f, \theta)(f=\omega/(2\pi))$ in the cell $(i_x, j_y) = (2,4)$ at (a) 6 LST 21 April 1998 and (b) 22 LST 7 May 1998.

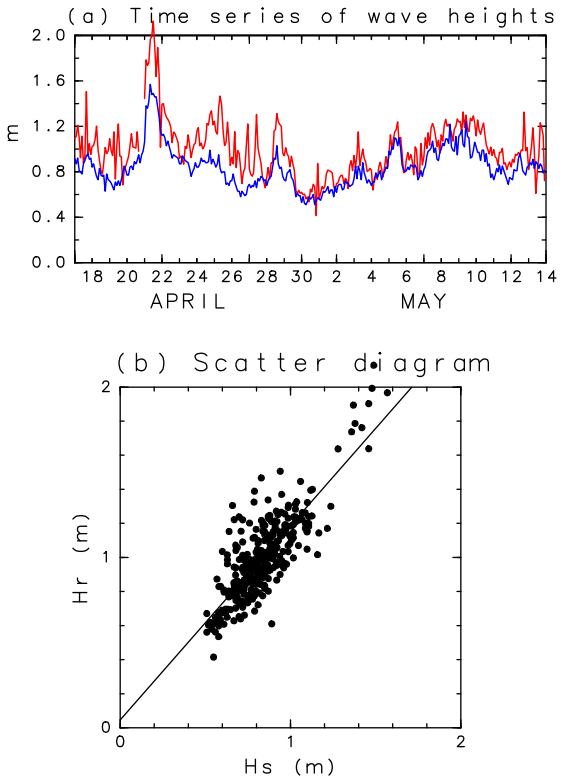

Figure 9. Comparison of radar-estimated wave heights (H_r) at the cell $(i_x, j_y) = (2, 4)$ and USW significant wave heights (H_s). (a) Time series (Blue: H_s, red: H_r); and (b) scatterplot between H_s and H_r. The linear line is the regression line.

Hashimoto et al., 2003; *Wyatt et al.*, 2011] can only estimate wave spectra for dual radar Doppler spectrum cells. This study demonstrates the advantages of the present method.

The wave spectra in the no-radar Doppler spectrum cell were estimated by interpolation or extrapolation from constraints 3 and 6 in section 2.1. The grid cell $(i_x, j_y) = (2, 4)$ was a no-radar Doppler spectrum cell only at 18 LST 12 May (Figure 7b), as well as from 18 LST to 22 LST 20 April. The radar-estimated wave height in the cell was 1.32 m, while the USW wave height was 0.79 m at 18 LST 12 May. The radar-estimated wave heights in the cell at 16 LST 12 May and 20 LST 12 May were both 0.99 m. The wave height at 18 LST 12 May was thus overestimated, probably due to the noise-contaminated Doppler spectra, because the radar-estimated wave height in the cell $(i_x, j_y) = (2, 2)$ was much larger than those in the surrounding cells at the time. Further improvement of the method for selecting Doppler spectra is necessary. The validity of wave estimation for no-radar Doppler spectrum cell should be explored further. The relationship between the accuracy of the radar-estimated wave height and $N_{cd}(i_x, j_y)$ remains unclear.

The Doppler spectra for constraints 1 and 2 in section 2.1 are the same in the present estimation, as indicated in equation (23). However, the first-order Doppler spectrum for constraint 1 in section 2.1 can be used even though the second-order scattering is contaminated by noise. This improvement will be explored.

The advantage of the method is that wave spectra can be estimated in both single and dual radar Doppler spectrum cells. In addition, the area for wave estimation can be set flexibly. The wave estimation area is set so that most of the cells are dual and single radar Doppler spectrum cells. The conditions for selecting the wave estimation area are less restrictive than those of other methods.

The advantage of the present method over the single radar method is that the area of wave estimation is also more flexible than that in the single radar method. If two radars are used, and the wave spectra are estimated by the single radar method for each radar, the area of wave estimation is wider. However, attempting to combine wave data from two radars is problematic. The wave data from each radar differ from each other, even in the radar overlapping coverage area. If the wave data in the overlapping coverage are corrected, wave data in the nonoverlapping coverage must be also corrected. The present method combines the wave data from multiple radars.

In addition, the method of quality control is improved compared with that in *Hisaki* [2009]. Control is performed for radar-estimated wave data in *Hisaki* [2009]. As a result, many radar-estimated wave data were discarded. Quality control was performed for the Doppler spectra in the present study. Even if only a few Doppler spectra for wave estimation are not good quality, the radar-estimated wave data will not be good quality. Therefore, the number of rejected wave data by the present method is smaller than that of the previous method [*Hisaki*, 2009].

The drawback of the current method is that it requires substantial computer memory, and, as a result, spatial and spectral resolutions are coarse. If we want to estimate wave spectra at higher spatial resolution, the wave estimation area must be narrower. This drawback can be resolved by advances in computer performance and memory.

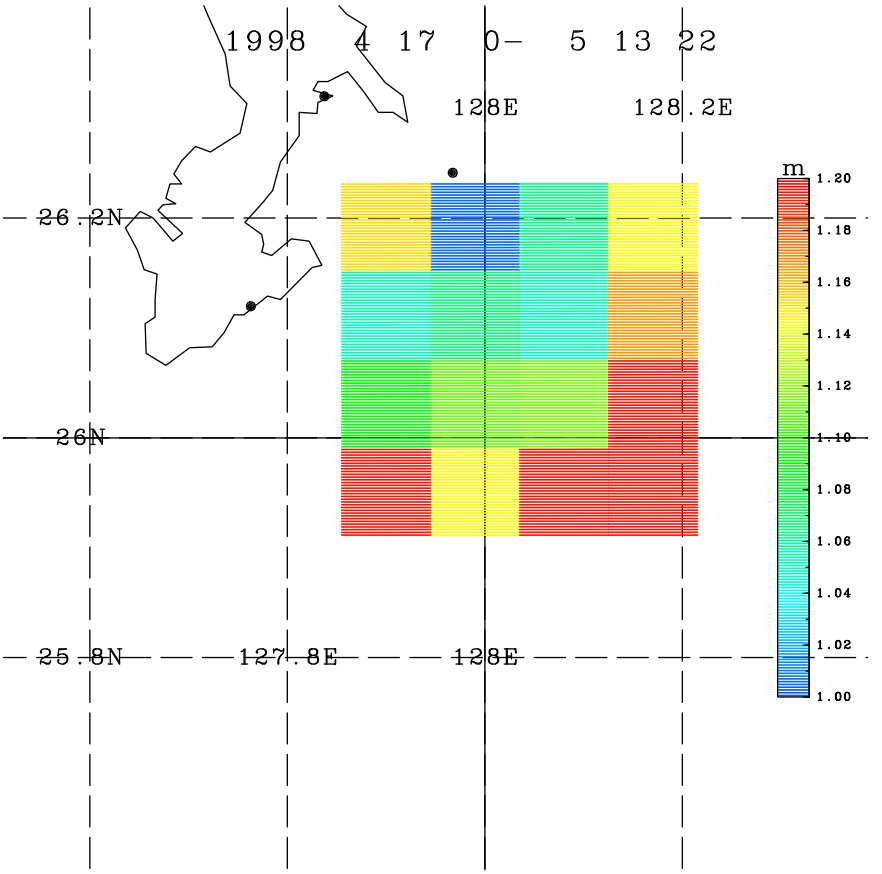

Figure 10. Mean radar-estimated wave heights during the observation period.

Our conclusions can be summarized as follows. We developed a method for estimating ocean wave spectra from HF radar by extending the method of *Hisaki* [2005, 2006, 2009, 2014] to multiple radar cases and regular wave estimation grids. A method for selecting Doppler spectra for wave estimation was also developed. The method was verified by comparing in situ observed wave height with the radar-estimated wave heights in a single radar Doppler spectrum cell in which the wave directional spectrum could not be estimated by the previous methods of other groups.

Acknowledgments

This study was supported by a grant-in-aid for scientific research (C-2) from the Ministry of Education, Culture, Sports, Science, and Technology of Japan (26420504). The GFD DENNOU Library (http://dennou.gaia.h.kyoto-u.ac.jp/arch/dcl/) was used for drawing figures. The Doppler spectra were provided from Okinawa Electromagnetic Technology Center, National Institute of Information and Communications Technology, Japan (http://okinawa.nict.go.jp/EN/). The wave data were provided from Coastal Development Institute of Technology, Japan (http://www.cdit.or.jp/). Comments from anonymous reviewers were helpful in improving the manuscript.

References

Barrick, D. E. (1977), The ocean wave height nondirectional spectrum from inversion of the HF sea-echo Doppler spectrum, *Remote Sens. Environ.*, *6*, 201–227, doi:10.1016/0034-4257(77)90004-9.

de Valk, C., A. Reniers, J. Atanga, A. Vizinho, and J. Vogelzang (1999), Monitoring surface waves in coastal waters by integrating HF radar measurement and modelling, *Coastal Eng.*, *37*, 431–453, doi:10.1016/S0378-3839(99)00037-X.

Hashimoto, N., L. R. Wyatt, and S. Kojima (2003), Verification of a Bayesian method for estimating directional spectra from HF radar surface backscatter, *Coastal Eng. J.*, *45*, 255–274, doi:10.1142/S0578563403000725.

Hisaki, Y. (1996), Nonlinear inversion of the integral equation to estimate ocean wave spectra from HF radar, *Radio Sci.*, *31*, 25–39, doi:10.1029/95RS02439.

Hisaki, Y. (2002), Short-wave directional properties in the vicinity of atmospheric and oceanic fronts, *J. Geophys. Res.*, *107*(C11), 3188, doi:10.1029/2001JC000912.

Hisaki, Y. (2005), Ocean wave directional spectra estimation from an HF ocean radar with a single antenna array: Observation, *J. Geophys. Res.*, *110*, C11004, doi:10.1029/2005JC002881.

Hisaki, Y. (2006), Ocean wave directional spectra estimation from an HF ocean radar with a single antenna array: Methodology, *J. Atmos. Oceanic Technol.*, *23*, 268–286, doi:10.1175/JTECH1836.1.

Hisaki, Y. (2007), Directional distribution of the short wave estimated from HF ocean radars, *J. Geophys. Res.*, *112*, C10014, doi:10.1029/2007JC004296.

Hisaki, Y., (2009), Quality control of surface wave data estimated from low signal-to-noise ratio HF radar Doppler spectra, *J. Atmos. Oceanic Technol.*, *26*, 2444–2461, doi:10.1175/2009JTECHO653.1.

Hisaki, Y. (2013), Classification of surface current maps, *Deep Sea Res., Part I*, *73*, 117–126, doi:10.1016/j.dsr.2012.12.001.

Hisaki, Y. (2014), Intercomparison of wave data obtained from single high-frequency radar, in-situ observation and model prediction, *Int. J. Remote Sens.*, *35*, 3459–3481, doi:10.1080/01431161.2014.904971.

Hisaki, Y., W. Fujiie, T. Tokeshi, K. Sato, and S. Fujii (2001), Surface current variability east of Okinawa Island obtained from remotely sensed and in-situ observational data, *J. Geophys. Res.*, *106*, 31,057–31,073, doi:10.1029/2000JC000784.

Howell, R., and J. Walsh (1993), Measurement of ocean wave spectra using narrow-beam HF radar, *IEEE. J. Oceanic Eng.*, *18*, 296–305, doi: 10.1109/JOE.1993.236368.

Japan Meteological Agency (1999), Annual report on ocean waves 1998, *Rep. 3*, Tokyo.

Lipa, B. J., and D. E. Barrick (1986), Extraction of sea state from HF radar sea echo: Mathematical theory and modeling, *Radio Sci.*, *21*, 81–100, doi:10.1029/RS021i001p00081.

Liu, Y., and R. H. Weisberg, (2005), Patterns of ocean current variability on the West Florida Shelf using the self organizing map, *J. Geophys. Res.*, *110*, C06003, doi:10.1029/2004JC002786.

Long, R., D. E. Barrick, J. L. Largier, and N. Garfield (2011), Wave observations from Central California: SeaSonde systems and in situ wave buoys, *J. Sensors*, *0112*, 1–18, doi:10.1155/2011/728936.

Wyatt, L. R. (1990), A relaxation method for integral inversion applied to HF radar measurement of the ocean wave directional spectra, *Int. J. Remote Sens.*, *11*, 1481–1494, doi:10.1080/01431169008955106.

Wyatt, L. R., J. J. Green, and A. Middleditch (2011), HF radar data quality requirements for wave measurement, *Coastal Eng.*, *58*, 327–336, doi:10.1016/j.coastaleng.2010.11.005.